# Supplementary Information

## Diagnostic criteria

Detailed inclusion and exclusion criteria for the diagnostic categories included in the ADNI sample can be found on the ADNI website (http://www.adni.loni.usc.edu/methods/). Briefly, healthy controls had MMSE scores between 24-30 (inclusive), a clinical dementia rating (CDR) = 0, were non-depressed, non-MCI, and non-demented. AD dementia patients had initial MMSE scores between 20-26 (inclusive), a CDR = 0.5 or 1.0, and fulfilled NINCDS-ADRDA criteria for clinically probable Alzheimer's disease (McKhann *et al.,* 1984).

In the BioFINDER study, inclusion criteria for healthy controls were: 1) aged ≥60 years old, 2) scored 28–30 points on the MMSE at the screening visit, 3) absence of cognitive symptoms as evaluated by a physician, 4) fluent in Swedish, 5) did not fulfill the criteria of MCI or any dementia; with the following exclusion criteria: 1) significant systemic illness making it difficult to participate, 2) presence of significant neurologic or psychiatric disease (e.g., stroke, Parkinson's disease, multiple sclerosis, major depression), 3) significant substance abuse. AD dementia patients met the DSM-IIIR criteria for dementia (American Psychiatric Association and American Psychiatric Association Work Group to Revise DSM-III, 1987) as well as the NINCDS-ADRDA criteria for AD (McKhann *et al.*, 1984). Exclusion criteria were significant systemic illness and significant alcohol abuse. AD diagnoses were confirmed by physicians who were blinded to any PET or CSF biomarker data.

In the present study, only clinically diagnosed AD dementia patients with biomarker evidence of cerebral amyloidosis were included in the patient samples, and cognitively normal controls with biomarker evidence of cerebral amyloidosis were excluded from the control samples. In ADNI data global amyloid status was determined using cortex-to-whole cerebellum $^{18}$F-florbetapir-PET standard uptake value ratios (SUVR) that have been calculated and made

available on the ADNI server by one of the ADNI PET core laboratories (Jagust Lab, UC Berkeley). Based on these values, amyloid-positivity was established using a recommended threshold of SUVR ≥ 1.11 (Landau *et al.*, 2013). In the BioFINDER data, global amyloid positivity was determined using cerebrospinal fluid measurements of Aβ42 with INNOTEST ELISAs (Fujirebio Europe, Ghent, Belgium) and an assay specific cut-off for abnormal CSF Aβ42 of <517 ng/L, as described previously (Palmqvist *et al.*, 2017).

## Imaging data acquisition

In the ADNI cohort, $^{18}$F-florbetapir-PET data were acquired on several different scanners at multiple sites. PET data was collected during a 50- to 70-minute interval following a 370 MBq bolus injection of $^{18}$F-florbetapir. MRI data were acquired on multiple 3T MRI scanners using scanner-specific T1-weighted sagittal 3D MPRAGE sequences. In order to increase signal uniformity across the multicenter scanner platforms, standardized image pre-processing is applied to all original ADNI PET and MRI scans. More detailed information on the different imaging protocols employed across ADNI sites and standardized image pre-processing steps for PET and MRI acquisitions can be found on the ADNI website (http://adni.loni.usc.edu/methods/).

In the BioFINDER cohort, $^{18}$F-flutemetamol-PET scans were performed as previously described (Palmqvist *et al.*, 2017) on a GE Discovery 690 PET scanner (General Electric Medical Systems) acquired as dynamic scans in LIST-mode 90–110 min post-injection of a bolus injection of $^{18}$F-flutemetamol. Low-dose CT-scans for attenuation correction were performed immediately prior to the PET scans. PET data were reconstructed into 4x5min frames using an iterative Vue Point HD algorithm with six subsets, 18 iterations with 3mm filter, and no time-of-flight correction. The scan frames were motion corrected using AFNI's 3dvolreg, time-averaged, and rigidly co-registered to a skull-stripped MRI scan. Structural MRI scans were acquired on a

Siemens Tim Trio 3T scanner (Siemens Medical Solutions, Erlangen, Germany) using a high resolution T1-weighted MPRAGE sequence (in-plane resolution = 1×1mm$^2$, slice thickness = 1.2mm, TR = 1950ms, TE = 3.37ms, flip-angle = 9°).

## Imaging data processing

ADNI imaging data were processed by using statistical parametric mapping (SPM8, Wellcome Trust Center for Neuroimaging) and the VBM8-toolbox (http://dbm.neuro.uni-jena.de/vbm/) implemented in MATLAB R2007a (MathWorks, Natick, MA) as described previously (Grothe and Teipel, 2016). MRI scans were automatically segmented into gray matter (GM), white matter, and cerebrospinal fluid partitions of 1.5mm isotropic voxel-size using the segmentation routine of the VBM8-toolbox. The resulting GM and WM partitions of each subject in native space were then high-dimensionally registered to an aging/AD-specific reference template from a previous study (Grothe *et al.*, 2013). Individual flow-fields resulting from the registration to the reference template were used to warp the GM segments and voxel-values were modulated for volumetric changes introduced by the high-dimensional normalization, such that the total amount of GM volume present before warping was preserved. Modulated warped GM segments were smoothed with a Gaussian smoothing kernel of 8mm full-width at half maximum (FWHM). All preprocessed GM maps passed a visual inspection for segmentation and registration accuracy. $^{18}$F-florbetapir-PET scans were rigidly coregistered to a skull-stripped version of the corresponding structural MRI scan and warped (without modulation) to the aging/AD-specific reference space using the deformation fields derived from the registration of the MRI scan. In order to limit signal spill over from surrounding tissue, voxels with a GM probability of less than 50% in the aging/AD template were removed from the warped PET scans. Preprocessed $^{18}$F-

florbetapir-PET scans were proportionately scaled by mean signal within the cerebellum, and smoothed with a Gaussian smoothing kernel of 8mm FWHM.

Imaging data of the BioFINDER cohort was processed at Lund University employing an in-house developed pipeline, which follows similar but not identical routines compared to the processing of the ADNI data described above. MRI scans were segmented and spatially normalized to standard MNI space using SPM12 and the CAT-toolbox (http://www.neuro.uni-jena.de/cat/). Normalized GM values were modulated for volumetric changes introduced by the high-dimensional normalization and smoothed with a Gaussian smoothing kernel of 8mm FWHM. $^{18}$F-flutemetamol-PET scans were time-averaged, coregistered to the corresponding MRI scan, and intensity normalized to reference signal in a composite reference region covering the whole cerebellum, the pons/brainstem region, and eroded cortical white matter. Reference regions were defined in the coregistered structural MRI scan using Freesurfer v6.0 (http://surfer.nmr.mgh.harvard.edu), including visual inspection for segmentation accuracy and manual correction of segmentation errors. PET images were finally spatially normalized to standard MNI space, employing spatial transformation parameters derived from a diffeomorphic registration of the co-registered MRI scan as implemented in the Advanced Normalization Tools (ANTs) toolbox (Avants *et al.*, 2014), and smoothed with a 8mm FWHM Gaussian filter.

## Additional analyses of *APP*-containing gene sets

In contrast to the data-driven replication of the association between regional patterns of *MAPT* expression and neurodegeneration, *APP* was not included among the genes identified in the genome-wide gene set enrichment analysis (GSEA) of the regional amyloid deposition pattern. Here, we explored the possibility that APP and its functional pathways may not be well represented in the analyzed gene set databases.

The *APP* gene is included in a total of 51 of the 1,533 examined gene sets (3,3%), covering functions related to G-protein coupled receptor signaling and peptide ligand binding, cellular homeostasis, and immune response (see Table S3). For comparison, the *MAPT* gene was included only in a slightly higher proportion of the examined gene sets (77/1,533, 5,0%), including the 4 gene sets of cluster N1 that reached significant FDR-corrected enrichment signal (Table 3) as well as similar gene groupings related to microtubule, cytoskeleton, cell/neuron development and differentiation, neurites, axons, and polarized growth (Table S4). Thus, underrepresentation of *APP* among the examined gene sets is not a likely explanation for the missing association in the GSEA analysis.

However, another possibility is that the *APP*-containing gene sets in the examined database may be biased to specific pathways and are not a comprehensive representation of *APP* functions. In order to explore whether there are any other gene networks that may link the *APP* gene to the identified amyloid-related pathways (Table 2), we used GeneMANIA software to compute an *APP* gene interaction network consisting of the 50 most highly interacting genes based on a composite gene-gene interaction profile from co-expressions, co-localizations, genetic interactions, pathways, physical interactions, and shared protein domains (Mostafavi et al., 2008; Montojo et al., 2010)(Fig. S1). This network was indeed found to be weakly linked to the A1 cluster of amyloid-related pathways by a single overlapping gene (*CALR*, calreticulin, an endoplasmatic chaperone). However, using GSEA this *APP*-specific gene interaction network did not show significant enrichment signal (NES = -0.85, p = 0.71).

Together, these analyses argue against a major analytic confound for *APP* in the GSEA of the amyloid deposition pattern, and corroborate the interpretation that APP and its related pathways play a comparably minor role for predicting amyloid levels in sporadic AD (Shinohara *et al.*, 2014).

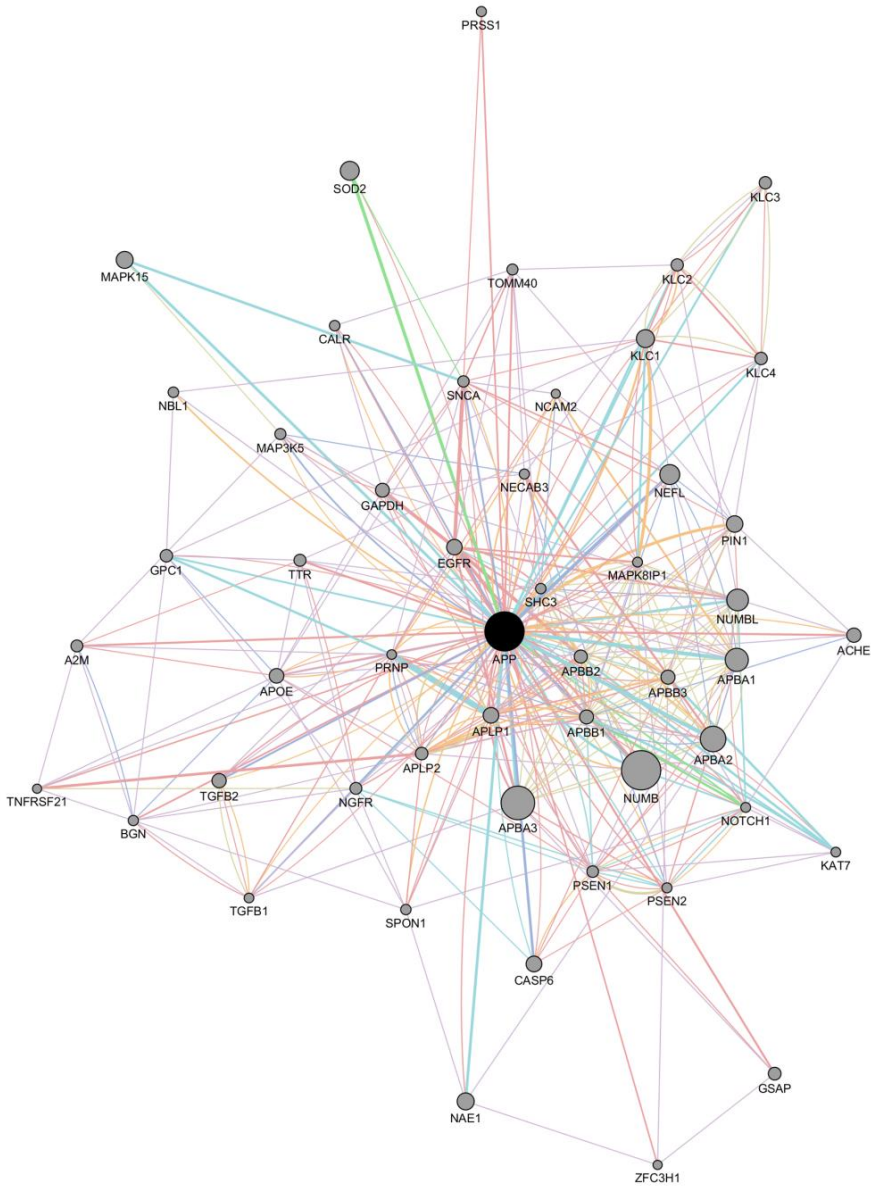


**Figure S1. *APP* gene interaction network.** APP-centered gene interaction network consisting of the 50 genes that most highly interact with *APP* (Mostafavi et al., 2008; Montojo et al., 2010).

## Extended discussion of the association between APOE expression and vulnerability to AD pathology

Given the close link between *APOE* variants and amyloid deposition (Kim *et al.*, 2009; Gonneaud *et al.*, 2016; Grothe *et al.*, 2017), the regional association of *APOE* expression with neurodegeneration instead of amyloid deposition is somewhat unexpected. Based on the known clearance function of APOE one could expect a negative spatial correlation between APOE levels and amyloid deposition, in a way that areas characterized by high/low APOE content (i.e. high/low clearance capabilities) should show low/high amyloid deposition. Indeed, previous studies found highest APOE levels in subcortical regions and the cerebellum, followed by medial temporal areas, and then neocortical areas (Xu et al., 1999; Riddell et al., 2008; Bekris et al., 2010), which inversely matches the regional distribution of amyloid deposition (Shinohara et al., 2014). The detailed cortical *APOE* expression profile from the Allen brain atlas that was analyzed in our study also replicates higher medial temporal compared to neocortical *APOE* expression levels (see Fig. S2). However, expression differences among distinct neocortical areas were generally not consistent with the regional pattern of amyloid vulnerability, as for example indicated by lowest *APOE* expression levels in the occipital pole which is also widely spared from amyloid deposition, and relatively high expression levels in the amyloid-vulnerable anterior cingulate cortex (see Figs. 1 and 5 of the manuscript). Together, these discrepancies result in a low overall spatial correlation between APOE expression and amyloid deposition of r=-0.09. By contrast, the overall cortical pattern of temporal>parietal>frontal>occipital *APOE* expression (see Fig. S2) more closely resembles the pattern of neurodegeneration-vulnerability, resulting in a (positive) spatial correlation of r=0.62 (see also the respective value in Table S2). Thus, the missing (inverse) spatial association between *APOE* expression and amyloid deposition may potentially be explained by the focus of our study on the cortical vulnerability patterns of AD.

Similar to our findings, a previous post-mortem study investigating the distribution of *APOE*-immunoreactive neurons across distinct occipito-temporal visual cortical areas in healthy older controls found that the differential *APOE* expression among these areas resembled their respective vulnerability to tau pathology (Einstein et al., 1998). Although purely speculative, a possible explanation for these differential associations with vulnerability to tau/neurodegeneration vs amyloid deposition may be that *APOE* expression in cortical areas differs from that in subcortical areas by a higher proportion of intraneuronal vs astrocytic APOE, which in turn is assumed to be more closely related to response to injury (i.e. plasticity) than to (astrocytic) clearance functions (Einstein et al., 1998; Xu et al., 1999).

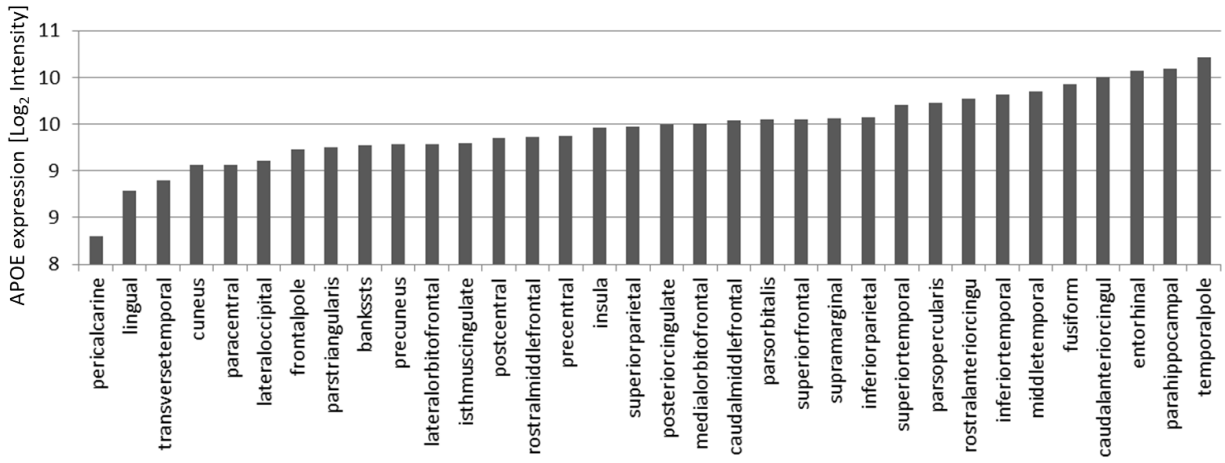


**Figure S2. APOE expression profile across cortical regions.**

## References

Avants BB, Libon DJ, Rascovsky K, Boller A, McMillan CT, Massimo L, et al. Sparse canonical correlation analysis relates network-level atrophy to multivariate cognitive measures in a neurodegenerative population. Neuroimage 2014; 84: 698-711.

Bekris LM, Galloway NM, Montine TJ, Schellenberg GD, Yu CE. APOE mRNA and protein expression in postmortem brain are modulated by an extended haplotype structure. American

journal of medical genetics Part B, Neuropsychiatric genetics : the official publication of the International Society of Psychiatric Genetics 2010; 153b(2): 409-17.

Einstein G, Patel V, Bautista P, Kenna M, Melone L, Fader R, et al. Intraneuronal ApoE in human visual cortical areas reflects the staging of Alzheimer disease pathology. Journal of neuropathology and experimental neurology 1998; 57(12): 1190-201.

Gonneaud J, Arenaza-Urquijo EM, Fouquet M, Perrotin A, Fradin S, de La Sayette V, et al. Relative effect of APOE epsilon4 on neuroimaging biomarker changes across the lifespan. Neurology 2016; 87(16): 1696-703.

Grothe M, Heinsen H, Teipel S. Longitudinal measures of cholinergic forebrain atrophy in the transition from healthy aging to Alzheimer's disease. Neurobiology of aging 2013; 34(4): 1210-20.

Grothe MJ, Teipel SJ. Spatial patterns of atrophy, hypometabolism, and amyloid deposition in Alzheimer's disease correspond to dissociable functional brain networks. Human brain mapping 2016; 37(1): 35-53.

Grothe MJ, Villeneuve S, Dyrba M, Bartres-Faz D, Wirth M. Multimodal characterization of older APOE2 carriers reveals selective reduction of amyloid load. Neurology 2017.

Kim J, Basak JM, Holtzman DM. The role of apolipoprotein E in Alzheimer's disease. Neuron 2009; 63(3): 287-303.

Landau SM, Breault C, Joshi AD, Pontecorvo M, Mathis CA, Jagust WJ, et al. Amyloid-beta imaging with Pittsburgh compound B and florbetapir: comparing radiotracers and quantification methods. J Nucl Med 2013; 54(1): 70-7.

McKhann G, Drachman D, Folstein M, Katzman R, Price D, Stadlan EM. Clinical diagnosis of Alzheimer's disease: report of the NINCDS-ADRDA Work Group under the auspices of

Department of Health and Human Services Task Force on Alzheimer's Disease. Neurology 1984; 34(7): 939-44.

Montojo J, Zuberi K, Rodriguez H, Kazi F, Wright G, Donaldson SL, et al. GeneMANIA Cytoscape plugin: fast gene function predictions on the desktop. Bioinformatics (Oxford, England) 2010; 26(22): 2927-8.

Mostafavi S, Ray D, Warde-Farley D, Grouios C, Morris Q. GeneMANIA: a real-time multiple association network integration algorithm for predicting gene function. Genome biology 2008; 9 Suppl 1: S4.

Palmqvist S, Scholl M, Strandberg O, Mattsson N, Stomrud E, Zetterberg H, et al. Earliest accumulation of beta-amyloid occurs within the default-mode network and concurrently affects brain connectivity. Nature communications 2017; 8(1): 1214.

Riddell DR, Zhou H, Atchison K, Warwick HK, Atkinson PJ, Jefferson J, et al. Impact of apolipoprotein E (ApoE) polymorphism on brain ApoE levels. The Journal of neuroscience : the official journal of the Society for Neuroscience 2008; 28(45): 11445-53.

Shinohara M, Fujioka S, Murray ME, Wojtas A, Baker M, Rovelet-Lecrux A, et al. Regional distribution of synaptic markers and APP correlate with distinct clinicopathological features in sporadic and familial Alzheimer's disease. Brain : a journal of neurology 2014; 137(Pt 5): 1533-49.

Xu PT, Gilbert JR, Qiu HL, Ervin J, Rothrock-Christian TR, Hulette C, et al. Specific regional transcription of apolipoprotein E in human brain neurons. The American journal of pathology 1999; 154(2): 601-11.